Pergamon

Int. J. Heat Mass Transfer. Vol. 40, No. 8, pp. 1743–1752, 1997

0017-9310/97 $17.00+0.00

PII: S0017-9310(96)00290-6

Mechanism of absorption enhancement by surfactant

H. DAIGUJI, E. HIHARA and T. SAITO

Department of Mechanical Engineering, The University of Tokyo, Hongo, Bunkyo-ku, Tokyo 113, Japan

(*Received* 22 *February* 1996 *and in final form* 30 *July* 1996)

Abstract—In absorption refrigeration technology, it is well known that the water vapor absorption into the lithium bromide (LiBr) aqueous solution is enhanced by the addition of surfactant. The Marangoni effect plays a role but its mechanism is not clearly understood yet. In the present study, the existence of instability due to Marangoni effect was investigated using the linear stability analysis, based on the salting out effect. Then the vapor absorption augmentation was estimated by the numerical simulation of cellular convection. Both theoretical results qualitatively agree well with the experimental ones. © 1997 Elsevier Science Ltd. All rights reserved.

1. INTRODUCTION

Vapor absorption into an absorbent solution is a key process in absorption heat pumps. For the absorption heat pump applications, improvement of absorber performance is one of the most important problems to be solved. In conventional systems, water and lithium bromide are used as the working fluid pair, and water vapor absorption into LiBr aqueous solution is enhanced by adding surfactant such as n-octanol or 2-ethyl-1-hexanol. The surface active material at the solution surface is playing an important role in this phase change process but there is less research concerning effect of surfactant.

Interphase mass transfer is often accompanied by cellular convection at the interface, induced by surface tension gradients which result from solute concentration gradients or temperature gradients. This phenomenon is called Marangoni instability. Brian [1] indicated that the convection causes spontaneous emulsification in liquid–liquid extraction systems, and even in gas–liquid systems, it enhances the mass transfer rate more than ten-fold.

In order to clarify the mechanism of absorption enhancement by surfactant, several researchers have investigated the relationship between surfactant and Marangoni instability. Kashiwagi *et al.* [2] explained that the interfacial turbulence is induced by the change of surface tension around the floating droplets of the surfactant. According to this explanation, the onset of interfacial turbulence requires excess amount of surfactant more than the solubility limit. Hozawa *et al.* [3] found that the surface tension of LiBr aqueous solution without surfactant increases with increase of LiBr concentration, on the other hand that with surfactant decreases with increase of LiBr concentration as shown in Fig. 1. This property is explained as follows. A part of surfactant molecules is dissolved in the solution, and the other surfactant molecules are adsorbed on the surface. When lithium bromide molecules are added to the solution, water molecules get to bind electrolyte ions, Li^+ and Br^-, instead of surfactant molecules because the hydration force with electrolyte ions is stronger than the bonding force with surfactant molecules. Consequently some surfactant molecules cannot be dissolved in the solution and are segregated to the solution surface. This phenomenon is called salting out. The segregated surface active molecules are adsorbed on the solution surface, and thus the surface tension of the solution decreases. Because the surface tension decreases with the concentration of lithium bromide, lithium bromide can be regarded as surface active material. Generally speaking, the surface active material has the property that the surface tension gradient with respect to the concentration is negative, and this property causes Marangoni instability. This mechanism was explained by Pearson [4] in the pioneering theoretical work on the Marangoni instability. Hozawa *et al.* [3] related the absorption augmentation by surfactant to Marangoni instability by considering the properties of surface tension. They concluded that the presence of an island of surfactant is not a necessary condition to initiate Marangoni convection. But the discussion was restricted to the origin of interfacial turbulence, and the quantitative discussion about the absorption augmentation was insufficient. Hihara and Saito [5] have studied the effect of surfactant on falling film absorption. They experimentally revealed that the absorption rate was dramatically enhanced by adding surfactant even if the amount of surfactant was below the solubility limit.

A theoretical understanding of Marangoni instability should lead ultimately to the prediction of its

NOMENCLATURE

c	lithium bromide (LiBr) concentration [wt%]
D	diffusivity [$m^2 s^{-1}$]
d	penetration depth [m]
g	gravitational acceleration [$m s^{-2}$]
h	height of solution [m]
k	wave number [m^{-1}]
L	latent heat [$J kg^{-1}$]
l	width of solution [m]
p	pressure [Pa]
t	temperature [K]
u	velocity in the x direction [$m s^{-1}$]
w	velocity in the z direction [$m s^{-1}$]
x	coordinate in the horizontal direction [m]
z	coordinate in the vertical direction [m].

Greek symbols

α	thermal diffusivity [$m^2 s^{-1}$]
β	coefficient of thermal expansion [K^{-1}]
β^+	volumetric coefficient due to lithium bromide concentration [$wt\%^{-1}$]
λ	thermal conductivity [$W m^{-1} K^{-1}$]
μ	viscosity [$Pa s^{-1}$]
ν	kinematic viscosity [$m^2 s^{-1}$]
ρ	density [$kg m^{-3}$]
σ	surface tension [$N m^{-1}$]
τ	time [s]
ω	angular frequency [s^{-1}]
ψ	stream function [$m^2 s^{-1}$].

Subscripts

i	vapor–liquid interface
0	value at $\tau = 0$.

occurrence and the enhancement ratio of the mass transfer. In the present study, for these predictions, the linear stability analysis and the numerical simulation were carried out, using the model proposed by Hozawa *et al.* [3]. The amount of water vapor, absorbed in a stagnant pool of LiBr aqueous solution, was experimentally measured and was compared with the calculated value.

2. GOVERNING EQUATIONS

The interfacial turbulence caused by Marangoni effect is considered in a steam absorption process. A schematic of the physical model and coordinate system is shown in Fig. 2. For two-dimensional, incompressible laminar flow conditions, conservation equations that describe the flow, and the heat- and mass-transport are written as follows:

$$\frac{\partial u}{\partial x}+\frac{\partial w}{\partial z}=0 \tag{1}$$

$$\frac{\partial u}{\partial \tau}+u\frac{\partial u}{\partial x}+w\frac{\partial u}{\partial z}=-\frac{1}{\rho}\frac{\partial p}{\partial x}+\nu\left(\frac{\partial^2 u}{\partial x^2}+\frac{\partial^2 u}{\partial z^2}\right) \tag{2}$$

$$\frac{\partial w}{\partial \tau}+u\frac{\partial w}{\partial x}+w\frac{\partial w}{\partial z}=-\frac{1}{\rho}\frac{\partial p}{\partial z}+\nu\left(\frac{\partial^2 w}{\partial x^2}+\frac{\partial^2 w}{\partial z^2}\right)+g\beta(t-t_0)+g\beta^+(c-c_0) \tag{3}$$

$$\frac{\partial t}{\partial \tau}+u\frac{\partial t}{\partial x}+w\frac{\partial t}{\partial z}=\alpha\left(\frac{\partial^2 t}{\partial x^2}+\frac{\partial^2 t}{\partial z^2}\right) \tag{4}$$

$$\frac{\partial c}{\partial \tau}+u\frac{\partial c}{\partial x}+w\frac{\partial c}{\partial z}=D\left(\frac{\partial^2 c}{\partial x^2}+\frac{\partial^2 c}{\partial z^2}\right) \tag{5}$$

where

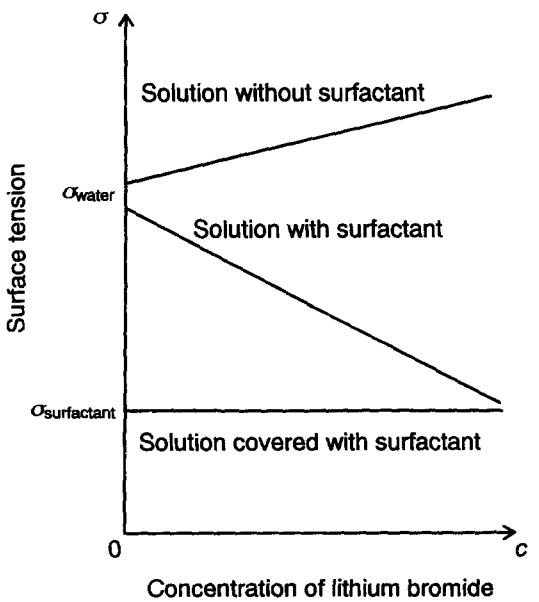

Fig. 1. Typical surface tension of LiBr aqueous solution with and without surfactant.

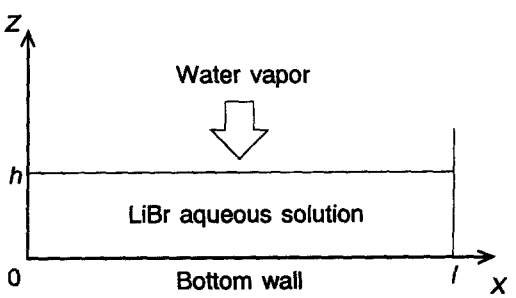

Fig. 2. Physical model and coordinate system.

$$\beta = -\frac{1}{\rho}\left(\frac{\partial\rho}{\partial t}\right)_{p,c} \quad \beta^+ = -\frac{1}{\rho}\left(\frac{\partial\rho}{\partial c}\right)_{p,t}. \tag{6}$$

The Boussinesq approximations that density variations are important only for the buoyancy terms, are assumed in equation (3). The boundary conditions at the vapor–liquid interface ($z = h$) are expressed by the following equations:

$$\mu\frac{\partial u}{\partial z} = \left(\frac{\partial\sigma}{\partial t}\right)\frac{\partial t}{\partial x} + \left(\frac{\partial\sigma}{\partial c}\right)\frac{\partial c}{\partial x} \tag{7}$$

$$w = 0 \tag{8}$$

$$\lambda\frac{\partial t}{\partial z} = -L\frac{D\rho}{c}\frac{\partial c}{\partial z} \tag{9}$$

$$t_i = \text{function}(c_i, p_i) \quad \text{(vapour–liquid equilibrium)}. \tag{10}$$

Equation (7) expresses that the shear stress is caused by surface tension gradients which result from solute concentration gradients and temperature gradients. This expression is based upon the salting out effect on the surface tension. Because the amount of surfactant dissolved in the solution is fairly closely related to the solute concentration, the amount of surfactant adsorbed on the surface and the resulting surface tension are directly correlated with the solute concentration beneath the surface. So, the surface tension can be expressed as a function of the solute concentration and the temperature. The coefficient $(\partial\sigma/\partial c)$ denotes the slope of the surface tension–LiBr concentration curve at steady state, and is assumed to be a negative constant because of the salting out effect. The partial differential of surface tension with respect to temperature, $(\partial\sigma/\partial t)$, is also a negative constant. Equation (9) denotes an energy balance concerned with phase change. In equation (10), a two-phase equilibrium state is assumed at a given vapor pressure during steam absorption.

3. LINEAR STABILITY ANALYSIS

3.1. *Differential equations*

In order to predict the occurrence of Marangoni instability, linear stability analysis was carried out. The present analysis is based on the frozen-profile assumption that the unperturbed temperature and concentration profiles are steady in time and are invariant with respect to the horizontal direction. The physical model is shown in Fig. 3. Soon after the start of absorption, the large thermal and concentration gradients in the vertical direction exist only near the surface, so only the region where z is larger than $h-d$ is the object of the study, and the region where z is smaller than $h-d$ is assumed to be equivalent to an adiabatic wall. The variables u, w, p, t, c are expressed like ϕ as the sum of the unperturbed value and an infinitesimal perturbation, as shown in equation (11):

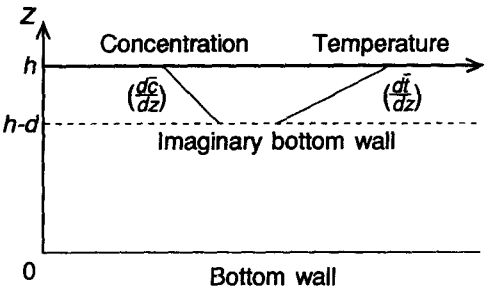

Fig. 3. Physical model.

$$\phi = \bar{\phi} + \phi'. \tag{11}$$

The infinitesimal perturbations in the z direction are assumed to be of the form:

$$\phi' = \Phi(z)\exp(ikx + \omega\tau) \tag{12}$$

where k and ω are the wave number and the complex angular frequency of disturbance, respectively, and Φ is the amplitude of the perturbation. By substitution of equation (11) into governing equations (1)–(5), the following differential equations are obtained:

$$(\mathrm{D}^2 - k^2)\left(\mathrm{D}^2 - k^2 - \frac{\omega}{\nu}\right)W = \frac{k^2 g}{\nu}(\beta T + \beta^+ C) \tag{13}$$

$$\left(\mathrm{D}^2 - k^2 - \frac{\omega}{\alpha}\right)T = \left(\frac{\mathrm{d}\bar{t}}{\mathrm{d}z}\right)\frac{1}{\alpha}W \tag{14}$$

$$\left(\mathrm{D}^2 - k^2 - \frac{\omega}{D}\right)C = \left(\frac{\mathrm{d}\bar{c}}{\mathrm{d}z}\right)\frac{1}{D}W \tag{15}$$

where D represents differentiation with respect to z ($\mathrm{D} = \mathrm{d}/\mathrm{d}z$). The corresponding boundary conditions on the vapor–liquid interface are expressed by the following equations:

$$\mu\mathrm{D}^2 W = k^2\left\{\left(\frac{\partial\sigma}{\partial t}\right)T + \left(\frac{\partial\sigma}{\partial c}\right)C\right\} \tag{16}$$

$$W = 0 \tag{17}$$

$$\lambda\mathrm{D}T = -L\frac{D\rho}{c_0}\mathrm{D}C \tag{18}$$

$$T = \left(\frac{\mathrm{d}t}{\mathrm{d}c}\right)C \tag{19}$$

where $(\mathrm{d}t/\mathrm{d}c)$ is the gradient of saturation temperature of LiBr aqueous solution with respect to the LiBr concentration at a given pressure, and assumed to be constant. The temperature and concentration gradients $(\mathrm{d}\bar{t}/\mathrm{d}z)$ and $(\mathrm{d}\bar{c}/\mathrm{d}z)$ in the vertical direction are assumed to be constant satisfying the following equation:

$$\lambda\left(\frac{d\bar{t}}{dz}\right) = -L\frac{D\rho}{c_0}\left(\frac{d\bar{c}}{dz}\right). \quad (20)$$

The following dimensionless groups are introduced.

$$z^* = \frac{z-(h-d)}{d} \quad D^* = \frac{d}{dz^*}(= Dd) \quad k^* = kd$$

$$w^* = \frac{wd}{\nu} \quad t^* = \frac{t}{t_0} \quad c^* = \frac{c}{c_0}$$

$$Pr = \frac{\nu}{\alpha} \quad Sc = \frac{\nu}{D} \quad A = \frac{LD\rho}{\lambda t_0} \quad B = \frac{dt^*}{dc^*}.$$

Other important dimensionless variables in this problem are the Marangoni number and the Rayleigh number

$$Ma = \frac{1}{\mu D}\left\{\left(\frac{\partial\sigma}{\partial t}\right)\left(\frac{dt}{dc}\right)+\left(\frac{\partial\sigma}{\partial c}\right)\right\}\left(\frac{d\bar{c}}{dz}\right)d^2 \quad (21)$$

$$Ra = -\frac{g}{\nu}\left\{\beta\left(\alpha\left(\frac{d\bar{t}}{dz}\right)+\frac{\beta^+}{D}\left(\frac{d\bar{c}}{dz}\right)\right\}d^4 \quad (22)$$

which represent the shear stress induced by surface tension gradients and the buoyant force, respectively. A marginal state separating stable states from unstable states is characterized by the condition $\omega = 0$. By substitution of $\omega = 0$ and dimensionless variables into equations (13)–(15) and equation (20), the following equations are obtained:

$$\{(D^{*2}-k^{*2})^3 + Ra\cdot k^{*2}\}W^* = 0 \quad (23)$$

$$(D^{*2}-k^{*2})T^* = \left(\frac{d\bar{t}^*}{dz^*}\right)Pr\cdot W^* \quad (24)$$

$$(D^{*2}-k^{*2})C^* = \left(\frac{d\bar{c}^*}{dz^*}\right)Sc\cdot W^* \quad (25)$$

where

$$\left(\frac{d\bar{t}^*}{dz^*}\right) = -A\left(\frac{d\bar{c}^*}{dz^*}\right). \quad (26)$$

The boundary conditions take here the following form:
at $z^* = 0$

$$D^*W^* = 0 \quad (27)$$

$$W^* = 0 \quad (28)$$

$$T^* = 0 \quad (29)$$

$$D^*C^* = 0 \quad (30)$$

at $z^* = 1$

$$D^{*2}W^* - k^{*2}C^*Ma/Sc = 0 \quad (31)$$

$$W^* = 0 \quad (32)$$

$$D^*T^* + AD^*C^* = 0 \quad (33)$$

$$T^* - BC^* = 0. \quad (34)$$

This system is always stable from the viewpoint of buoyant effect because the upper solution is lighter than the lower solution, namely, the Rayleigh number is always negative. But this system may be unstable from the viewpoint of Marangoni effect. We are facing here an eigenvalue problem for Ma at the marginal state. In other words, only for particular values of Ma, we will find a non-vanishing solution W^*, T^* and C^*, satisfying the boundary conditions (27)–(34) for a given k^*.

3.2. *Results and discussion*

In Fig. 4, the curves of neutral stability are plotted on a plane of Marangoni number Ma vs the dimensionless wave number k^* at different Rayleigh numbers, Ra. Each curve separates a stable region to the left from an unstable one to the right. As the concentration gradient $(d\bar{c}/dz)$ in the z direction increases, the Marangoni number becomes larger, and the Rayleigh number becomes smaller. Therefore the system becomes unstable from the viewpoint of Marangoni effect and becomes stable from the viewpoint of buoyant effect. When penetration depth d is very small, namely when the Rayleigh number is near to zero, the buoyant effect is negligible because the curves of neutral stability converge. Figure 4 also indicates the existence of critical wave number which corresponds to the minimum Marangoni number. The ratio of the critical wave lengths to the penetration depth was calculated to be 0.5–0.7. A quantitative discussion about this linear stability analysis is still insufficient, but the qualitative trend agrees well with the experimental results.

4. NUMERICAL SIMULATION OF CELLULAR CONVECTION

4.1. *Method of solution*

In order to investigate the motion of the cellular convection caused by Marangoni effect and to predict its effect upon the mass transfer rate, the governing equations (1)–(10) were solved using SIMPLE algorithm of Patankar [6]. The calculation region is the same as on Fig. 2. Both sides and bottom wall are adiabatic. In the beginning, the solution is at rest, and heat and mass are transferred only by molecular diffusion. A local concentration variation is given near the center of vapor–liquid interface, at $\tau = 0.1$ s, for the initiation of fluctuation.

A grid of 78×42 control volumes was used. The grid interval in the x direction, Δx, was 1.0 mm. The grid interval in the z direction, Δz, was non-uniform, with the grid points placed at geometrically decreasing distances in the regions next to interface, where large velocity, temperature and concentration gradients were expected. The grid intervals in the z direction were determined so narrow that the calculated value of absorbed mass did not change even if the narrower grid intervals were selected. The values of temperature and concentration at the vapor–liquid interface were

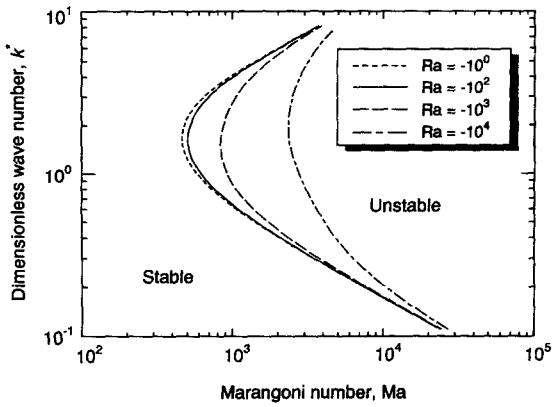

Fig. 4. Neutral stability curves for $A = 0.266$, $B = 0.0449$, $Pr = 19$, $Sc = 1650$.

Table 1. Thermophysical properties and parameters

D	1.43×10^{-9}	[$m^2 s^{-1}$]	ρ	1.624×10^3	[$kg m^{-3}$]
g	9.8	[$m s^{-2}$]	$(\partial\sigma/\partial c)$	-6.4×10^{-4}	[$N m^{-1} wt\%^{-1}$]
L	2.568×10^6	[$J kg^{-1}$]	$(\partial\sigma/\partial t)$	-2.1×10^{-4}	[$N m^{-1} K^{-1}$]
α	1.235×10^{-7}	[$m^2 s^{-1}$]	c_0	55.22	[wt%]
β	3.645×10^{-4}	[K^{-1}]	h	0.010	[m]
β^+	-1.109×10^{-2}	[$wt\%^{-1}$]	l	0.076	[m]
λ	4.38×10^{-1}	[$W m^{-1} K^{-1}$]	p_i	2.315×10^3	[Pa]
μ	3.83×10^{-3}	[$kg m^{-1} s^{-1}$]	t_0	303	[K]
ν	2.358×10^{-6}	[$m^2 s^{-1}$]	$\Delta\tau$	0.01	[s]

$t_i = 1.458c_i + 242.6$ at 2.315×10^3 [Pa] equation (10)

explicitly renewed at each time step, and the time interval was taken small enough to maintain Courant number below 1.0.

4.2. *Results and discussion*

The thermophysical properties and parameters used in the calculation are listed in Table 1. Figure 5 shows the stream lines and the contour plots of temperature and LiBr concentration for the first 3 min. After a local concentration variation is given near the center ($x \cong l/2$) of vapor–liquid interface, the fluctuations of flow velocity, temperature and concentration are induced, and grow to bulk convective flows. Soon the temperature and concentration gradients in the vertical direction become small, then surface tension gradients at the surface become small, which means that the shear stresses at the surface become small. Therefore the flow velocity gets slower and the convective cells become large. After 3 min, the convective cells are restricted in a layer near the surface because of buoyancy due to mixing with the absorbed water vapor. This trend agrees well with the experimental observation.

Figure 6 shows the velocity vectors, absorption rate and concentration at the vapor–liquid interface for 7.5–10.0 s. At a point where the surface is expanding, the LiBr concentration is high, and the absorption rate is also high. The higher absorption rate tends to lower the LiBr concentration and to raise the surface tension relatively, opposing the expansion of the surface. The reason why the surface tension increases with decrease of LiBr concentration is explained by the salting out effect as shown in Fig. 1. On the other hand, where the surface is contracting, the LiBr concentration is low, and the absorption rate is also low. The lower absorption rate tends to raise the LiBr concentration and to lower the surface tension relatively with the same reason, opposing the surface contraction. Therefore the steady convective cells cannot be formed and the solution moves right and left, changing the direction periodically as shown in Fig. 6. A flow pattern like this is in accordance with the experimental observation. Furthermore, Vliet and Cosenza [7] indicated that as for the LiBr aqueous solution with surfactant, longitudinal waves were observed on falling films along horizontal tubes, absorbing water vapor, and the characteristic waves whose directions were perpendicular to the flow direction were observed only when surfactant was added. The results of this numerical simulation can explain that the waves are caused by Marangoni effect. The calculated values of mass transfer rate will be compared with experimental ones in the next section.

5. EXPERIMENT

5.1. *Experimental apparatus*

The experimental apparatus shown in Fig. 7 consists of an evaporator, an absorber, and a data acqui-

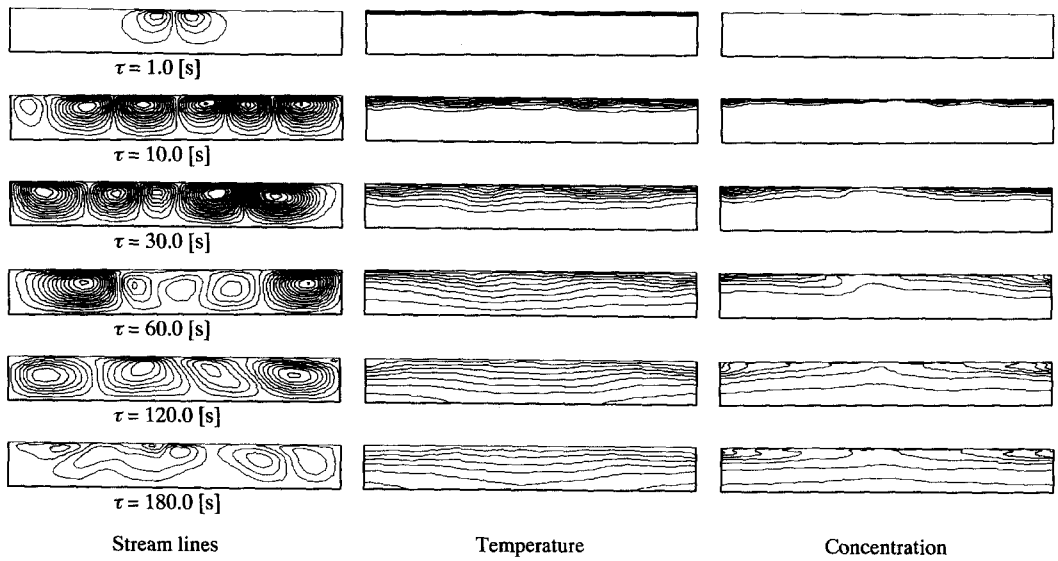

Fig. 5. Stream lines and contour plots of temperature and LiBr concentration ($\Delta\psi = 1.0 \times 10^{-6}$ m^2 s^{-1}, $\Delta t = 2.0$ K, $\Delta c = 0.2$ wt%).

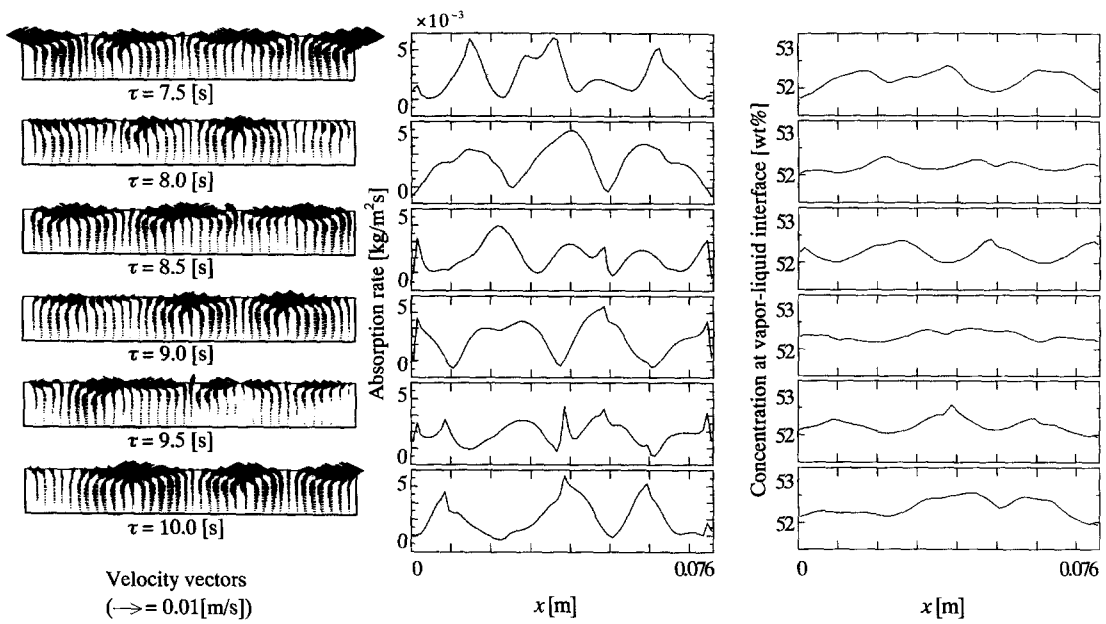

Fig. 6. Flow pattern, local absorption rate and interfacial concentration.

sition system. In order to measure the amount of absorbed water vapor, a plastic dish ($\phi = 86$ mm) containing the absorbent solution was suspended from a thin beam load cell, installed inside the absorber. As the weight of the absorbent solution increases, the beam deflection also increases. The beam deflection is measured by a strain gauge struck on the load cell. The voltage output from the load cell is proportional to the weight of the absorbent solution. The signal from the load cell was logged in the recorder through an amplifier.

Experiments were performed according to the following procedure. Predetermined volume of LiBr aqueous solution with or without surfactant was poured into the empty dish suspended from the load cell. Then all the system was covered up and evacuated by the vacuum pump. The valve was opened for supplying water vapor to the absorber. The data from load cell were logged in the recorder every 2.5 s.

5.2. *Experimental results and comparison with the calculated results*

The typical experimental conditions are shown in Table 2. The initial saturation pressures of the LiBr

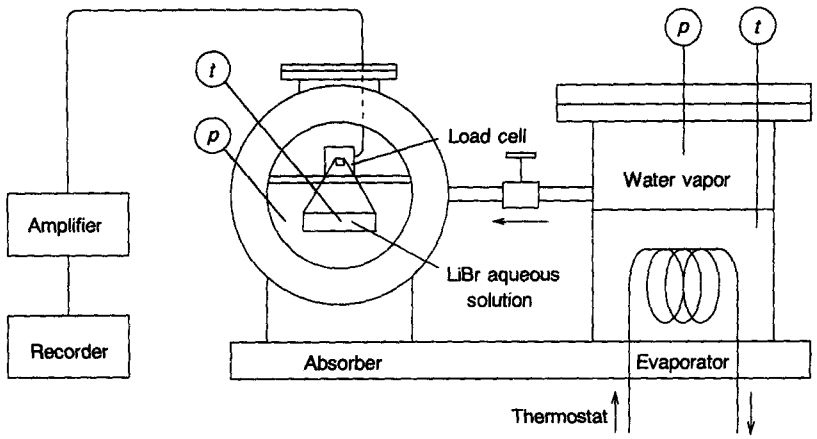

Fig. 7. Schematic experimental apparatus.

Table 2. Experimental conditions

Evaporating temperature	20°C	Depth of solution	10 mm
Initial temperature of solution	30°C	Kind of surfactant	n-octanol
Initial LiBr concentration	55 wt%	Concentration of surfactant	25 ppm

solution and the evaporator are 0.402 kPa and 2.315 kPa, respectively. This pressure difference is the primary driving force for the vapor absorption into the LiBr aqueous solution. n-Octanol was used as surfactant, which is often used in commercial absorption refrigerating machines. Repeatability of experiments was examined to assess accuracy of measurement. In Fig. 8 variations of measured values of absorbed mass vs time are plotted for three runs under the same conditions in the following two cases: (1) without surfactant; (2) with surfactant. The results show that in case (1), measured values are mostly within the range of average values ± 0.05 g, on the other hand, in case (2), the uncertainty of the data tends to be larger than case (1). In the following experiments, experiments were carried out three times under the same conditions, and average values of three runs are plotted in each figure.

Figure 9 shows the effect of the surfactant concentrations on vapor absorption augmentation. When the concentration of surfactant is more than 25 ppm, the measured values of absorbed mass are almost the same. The minimum concentration of n-octanol under which interfacial turbulence occurs is much weaker than its solubility limit, which is about 100 ppm, and if the concentration of surfactant is more than a certain value, which is supposed to be between 10 and 25 ppm, it does not affect the absorption enhancement.

Figure 10 shows difference of several kinds of surfactant on vapor absorption augmentation. The number of carbon atoms in normal alcohol used as sur-

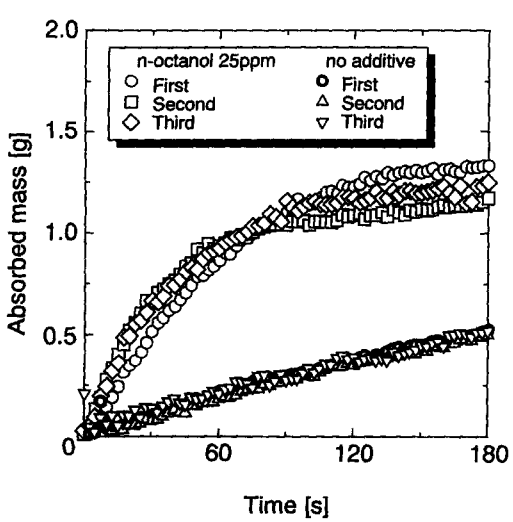

Fig. 8. Repeatability.

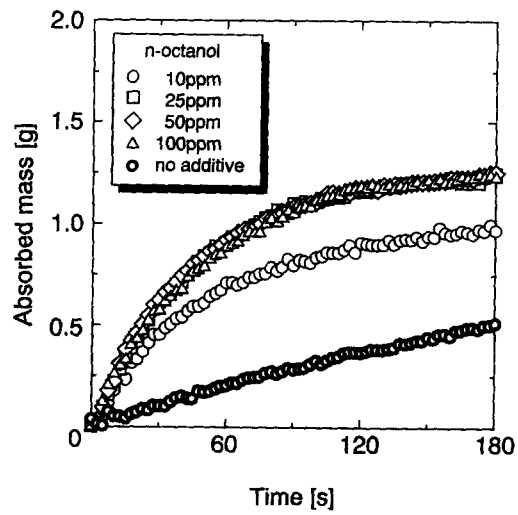

Fig. 9. The effect of concentration of surfactant on vapor absorption augmentation.

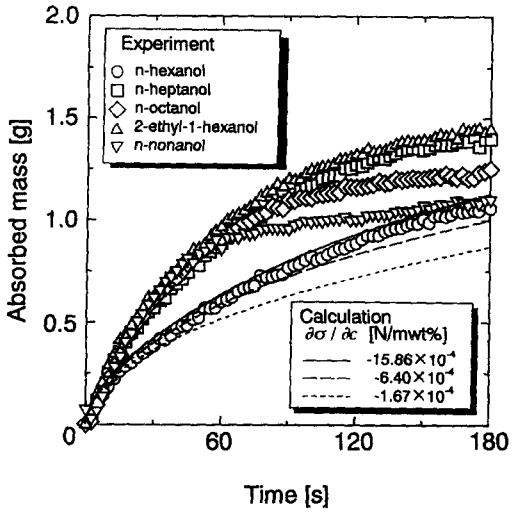

Fig. 10. Difference of the kind of surfactant on vapor absorption augmentation.

factant in the experiment was six to nine. 2-ethyl-1-hexanol is an isomer of n-octanol. The concentration of surfactant was 25 ppm. Except n-hexanol, other alcohols enhanced the absorption rate as well as n-octanol. The calculated results are also shown in Fig. 10. In order to investigate the effect of the value of $(\partial\sigma/\partial c)$, it was set to -0.167 mN m^{-1} wt%$^{-1}$, -0.64 mN m^{-1} wt%$^{-1}$ or -1.586 mN m^{-1} wt%$^{-1}$. The value of -0.64 corresponds to 65 ppm of n-octanol which was tested by Hozawa *et al.* [3]. The values of -0.167 and -1.586 were determined, as the values of $(\partial\sigma/\partial t)(dt/dc)+(\partial\sigma/\partial c)$ were half and twice of the case of 65 ppm, respectively. The larger the slope of surface tension–LiBr concentration curve is, the larger the calculated value of absorbed mass is. But the calculated values are smaller than the measured ones.

Figure 11 shows variation of absorbed mass with depth of solution. Within 3 min, in the case without additive, the absorbed mass was almost the same in every depth. On the other hand, in the case with additive, the absorbed mass was different with depth. The calculated values are also shown in Fig. 11. The deeper the solution is, the larger the value of absorbed mass is. Both experimental and calculated results show the same tendency, but the calculated values are smaller than the measured ones.

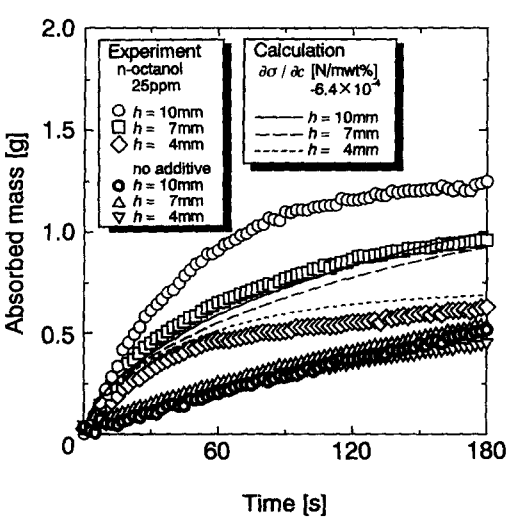

Fig. 11. Variation of absorbed mass with depth of solution.

6. DISCUSSION

In the comparison between the calculated and the measured values on the absorbed mass, the calculated values tend to be smaller than the measured ones in general. In the present numerical simulation, two equilibrium states, namely, vapor–liquid equilibrium at a given vapor pressure and adsorption equilibrium were assumed at the interface. The former is concerned with phase change process, and the latter is concerned with adsorption of surfactant. Especially the latter is the key hypothesis, and the salting out effect is based on this hypothesis. The adsorption hypothesis of surfactant makes it unnecessary to treat the concentration of surfactant as expressed in equation (7). In order to more correctly predict the enhancement ratio of mass transfer, it is important to investigate these two physical events, that is, phase change process and salting out, in more detail.

6.1. *Phase change process*

In the present numerical simulation, the vapor–liquid interface was assumed to be in an equilibrium state at a given vapor pressure during steam absorption. But in these experimental conditions, at initial state, the saturation pressure of the LiBr solution and the vapor pressure are 0.402 kPa and 2.315 kPa, respectively. This pressure difference is the primary driving force for the vapor absorption into the LiBr aqueous solution. In order to investigate the validity of the constitutive equations concerned with phase change process, equation (9) and equation (10), the amount of water vapor, absorbed in a stagnant pool of LiBr aqueous solution without surfactant, was both experimentally and numerically obtained. By the way, the saturation pressure of the solution is considered to be a function of the temperature and the concentration. Even if the initial saturation pressure is the same value, the phase change process may be different with the initial LiBr concentration and the initial temperature. The effect of the initial LiBr concentration on the absorbed mass is illustrated in Fig. 12. The initial temperature was accordingly predetermined as the initial saturation pressure was the same value (0.402 kPa). In the calculation, different thermophysical properties and equation (10) were used according to each condition.

When the LiBr concentration is low, the calculated mass agrees with the measured one. But as the LiBr concentration gets higher, the difference between the calculated and the measured mass gets larger. The reason is supposed that as the LiBr concentration gets

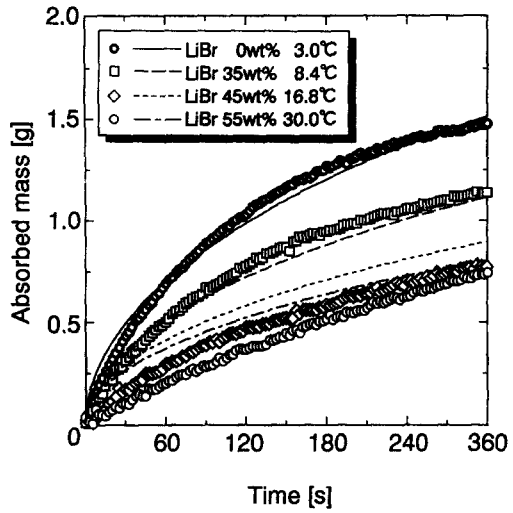

Fig. 12. The effect of superheat of the solution on absorbed mass for the initial saturation pressure 0.402 kPa and the vapor pressure 2.315 kPa.

higher, the thermal resistance of absorption in vapor phase gets larger because, if the LiBr aqueous solutions with different concentrations have the same saturation pressure, the highly concentrated solution is hotter. If the thermal resistance is considered in the vapor phase, the calculated values may approach to the measured ones. The further research on the effect of thermal resistance in the vapor phase on the phase change process is expected.

6.2. *Salting out*

In the present numerical simulation, we analyzed the fluid motion and the heat and mass transfer taking place in such a large absorption vessel as used in the experiments. Therefore the grid interval in the x direction, Δx, was determined to be quite large. But soon after the start of absorption, because the diffusivity of the solute is very small, the penetration depth, d, is very thin. According to the results of linear stability analysis, based on the salting out effect, the wave length shorter than the penetration depth is unstable for some conditions, so the small-scale convective cells may exist in a thin layer near the surface. Particularly when the large thermal and concentration gradients in the vertical direction exist near the surface, the small-scale convective cells may affect the absorption enhancement. The further research on the effect of the small-scale convective cells is expected.

Application of the present model based on the salting out effect to the problem in which the concentration of surfactant is more than the solubility limit is discussed. The gradient of the surface tension–LiBr concentration curve, $(\partial\sigma/\partial c)$ is different with the kind of surfactant added to the solution and is also different with its concentration. Because the object of the present study is the LiBr aqueous solution with surfactant whose concentration is below the solubility limit, the value of $(\partial\sigma/\partial c)$ is assumed to be invariant with the concentration of surfactant unless its concentration was quite low. The appropriateness of this assumption was certified by the experiment to investigate the effect of the concentration as shown in Fig. 9. When the concentration of surfactant exceeds the solubility limit, it is difficult to explain Marangoni instability only by the present model due to the existence of the droplets of surfactant. In this case, the present model is valid, but the model proposed by Kashiwagi *et al.* [2] may be also applicable. When most of the surface is covered with the surfactant, the value of $(\partial\sigma/\partial c)$ is almost zero as shown in Fig. 1, and the calculated absorbed mass is reduced. This result agrees with other experiments (Kashiwagi *et al.* [2] and Hozawa *et al.* [3]).

The comparisons between the experimental results and theoretical ones show that when absorption enhancement is small, the measured values of mass absorbed agree well with the calculated ones, but when strong interfacial turbulence occurs and absorption rate is dramatically enhanced, the measured values of mass absorbed do not agree well with the calculated ones. The main reason of this discrepancy is supposed that when strong interfacial turbulence occurs, the flow is so much faster than the adsorption or desorption rate of surfactant that the distribution of concentration of surfactant in the adsorption layer may not be in accordance with that of LiBr concentration beneath the surface. Many phenomena caused by the Marangoni effect can be reasonably explained by the salting out effect, but in order to more correctly predict the occurrence of Marangoni instability and the enhancement ratio of mass transfer, especially when the departure from equilibrium is large or the concentration of surfactant exceeds the solubility limit, the theoretical understanding of the dynamic properties or other characteristic properties of surfactant itself is inevitable.

7. CONCLUDING REMARKS

For the prediction of the occurrence of Marangoni instability and the enhancement ratio of mass transfer, the linear stability analysis and the numerical simulation were carried out, using the model based on the salting out effect. The amount of water vapor absorbed in a stagnant pool of the LiBr aqueous solution was experimentally measured and was compared with the calculated value. Following conclusions can be drawn from this study.

(1) The existence of critical wave number was indicated by the linear stability analysis.
(2) In the numerical simulation, cellular convection caused by the Marangoni effect can be reasonably explained by the salting out effect.
(3) In the experiment, the effects of the concentration of surfactant, the kind of surfactant and the depth of solution on absorption enhancement were quantitatively revealed. When absorption

enhancement is not large, the measured values of mass absorbed agree well with the calculated ones.

(4) When surfactant is added, the gradient of surface tension with respect to LiBr concentration, $(\partial\sigma/\partial c)$ changes to negative, because of the salting out effect. The larger the gradient is, the more effective the surfactant is.

Acknowledgements—The authors wish to acknowledge the financial support by Tokyo Gas Co. and the help of Ebara Co.

REFERENCES

1. P. L. T. Brian, Effect of Gibbs adsorption on Marangoni instability, *A.I.Ch.E. Jl* **17,** 765–772 (1971).
2. T. Kashiwagi, Y. Kurosaki and H. Shishido, Enhancement of vapor absorption into a solution using Marangoni effect, *Trans. JSME* **B51,** 1002–1009 (1985).
3. M. Hozawa, M. Inoue, J. Sato, T. Tsukada and N. Imaishi, Marangoni convection during steam absorption into aqueous LiBr solution with surfactant, *J. Chem. Engng Japan* **24,** 209–214 (1991).
4. J. R. A. Pearson, On convection cells induced by surface tension, *J. Fluid Mech.* **4,** 489–500 (1958).
5. E. Hihara and T. Saito, Effect of surfactant on falling film absorption, *Int. J. Refrig.* **16,** 339–346 (1993).
6. S. V. Patankar, *Numerical Heat Transfer and Fluid Flow* (Edited by W. J. Minkowycz and E. M. Sparrow). Hemisphere, Washington, D.C. (1980).
7. C. Vliet and F. B. Cosenza, Absorption in falling water/LiBr films on horizontal tubes, *ASHRAE Trans.* **96,** 693–701 (1990).